CONSTRAINING NUMERICAL GEODYNAMO WITH SURFACE OBSERVATIONS: A GEOMAGNETIC DATA ASSIMILATION APPROACH

Weijia Kuang[(1)], Zhibin Sun[(2)], Andrew Tangborn[(1)], Don Liu[(2)], Weiyuan Jiang[(2)]

[(1)] NASA Goddard Space flight Center, Greenbelt, Maryland, USA, Email: Weijia.Kuang-1@nasa.gov
[(2)] JCET, UMBC, Baltimore, Maryland, USA, Email: Sunzhib1@umbc.edu

ABSTRACT

Numerical geodynamo models have been focused on understanding qualitatively the mechanisms of generating and maintaining a magnetic field in the Earth's core. In this paper, we discuss our effort on using surface geomagnetic observations to constrain the numerical model, with the approach of data assimilation, aiming at understanding how do the models respond to the constraints. Using an optimal interpolation algorithm with 100 years of surface observations and with synthetic data for a much longer period (one magnetic free decay time τ_d), we found that the poloidal field in the core responds positively to the observational constraints: the errors between the truth and the prediction near the core-mantle boundary decrease with the spin-up time. Other physical variables also respond to the constraint. However, appropriate assessment of the response needs further research in geomagnetic data assimilation, in particular on more optimal algorithms to create an analysis from a model prediction and surface observations.

1. INTRODUCTION

Over the past decade, numerical dynamo models have been developed to simulate convective processes in the Earth's fluid outer core, which is believed to generate and maintain the core magnetic field (hereafter we call this intrinsic field the geomagnetic field). For a recent review on the work in this field, we refer the reader to [1].

However, most of the numerical modeling efforts have been towards the qualitative understanding of the properties of the field and flow with respect to give parameters that describe the physical and geometric properties of the model system. These include the Rayleigh number R_{th} (that describes the buoyancy force strength relative to the Coriolis force), the magnetic Rossby number R_o that measures the fluid inertia respect to the Coriolis force, and the Ekman number E that measures the fluid viscosity relative to the Coriolis force.

Regardless the values of these parameters and other approximations applied in the model, all models display some characteristics of the observed geomagnetic data, e.g. a dominantly dipolar poloidal field at the core-mantle boundary (CMB), a consistent "west-ward drift" of the poloidal field, and occasional reversals of the field.

But, numerical model results also show that, despite the similarity of the poloidal field at the CMB, it, and other variables can be very different inside the core [2]. This result, in addition to deserving further numerical investigation, indicates the importance and the urgency of applying surface geomagnetic observations to constrain numerical geodynamo models.

We intend to address this issue via data assimilation, which has been widely used in atmospheric [3] and oceanic modeling [4]: using observations to improve numerical models so that better estimation of the true physical states can be made. Our goals are clear: by examining the error (the difference between the model output and the true physical state in the core) variations, we wish to identify appropriate physical approximations applied in numerical models. We also wish to use the improved numerical model, together with the past and current surface observations, to better predict future geomagnetic secular variation.

The particular technique we intend to use for our study is the sequential data assimilation technique. The simplest explanation is as follows. Assume $\mathbf{x}$ is the state variable vector of the system in consideration. At time t_k, when the observation $\mathbf{x}^o$ and the model forecast $\mathbf{x}^f$ are made, an analysis $\mathbf{x}^a$ is constructed via the formulation

$$\mathbf{x}^a = \mathbf{x}^f + \mathbf{K}\left(\mathbf{x}^o - \mathbf{H}\mathbf{x}^f\right), \qquad (1)$$

where $\mathbf{K}$ is the gain matrix, and $\mathbf{H}$ is the observation operator. The analysis $\mathbf{x}^a$ is then used as the initial state at t_k for numerical simulation. The simulation results in the subsequent time are the model forecast based on the initial state $\mathbf{x}^a$ at t_k. The process (1) shall be repeated at the next time t_{k+1}, when another observation is made. By repeating this process, the model output should be pulled closer to the true state of the system.

There are many problems remain to be solved. It is not clear whether the sparse surface observation (in terms of the spectral coefficients of the state variables and of the observation history) could be sufficient to influence the whole model (e.g. whether the observation constraint is sufficiently strong to change the model output). In

addition, due to orders of magnitude differences between parameters used in the numerical models and those appropriate for the Earth's core, it is not certain whether the models can be pulled at all closer to the true physical state in the Earth's core. Furthermore, to obtain an optimal gain matrix **K** (e.g. via ensemble covariance analysis), the computing resource required for such simulation can be several orders of magnitude more than that for purely numerical dynamo modelling (which can easily reach beyond the capacity of the currently available computing systems).

Given the limitation of the surface geomagnetic observation and of the numerical modelling, and the extremely demanding computing resource, creative approaches are necessary for us to make progress in this research. In the following sections, we shall report our progress in this research and the potentials for the on-going effort in geomagnetic data assimilation.

2. OPTIMAL INTERPOLATION AND ENSEMBLE COVARIANCE ALGORITHMS

There are different algorithms to calculate the gain matrix **K**. In our study, we choose two methods: One is the optimal interpolation algorithm (OI). The other is based on ensemble covariance analysis. The philosophy of our approaches is simple. We wish to start with a simple algorithm which is mathematical consistent, e.g. ensuring continuity of the state variables and their spatial derivatives. But it does not depend on model details, e.g. numerical techniques, resolutions, parameters, etc. This could permit us to analyze responses of the model to the constraints from surface observations without substantial increase in computation demand. However, this simple approach is likely not optimal, since it does not incorporate available model information.

The ensemble covariance analysis is more sophisticated. It depends on the details of the model used for data assimilation, thus, in comparison with the first approach it is more "optimal". However, this algorithm depends on ensemble sizes in analysis. In general, the ensemble size can be above 100, thus increasing the CPU time by two orders of magnitude. For this reason, we intend to implement this approach after better understanding of the error dynamics of the system.

We introduce two parameters in the assimilation algorithms: one is the magnetic field scaling factor α and the other is the spatial correlation length r_c. The scaling factor α is defined such that the analysis is made with the scaled observations, e.g. (1) is modified as

$$\mathbf{x}^a = \mathbf{x}^f + \mathbf{K}\left(\alpha\mathbf{x}^o - \mathbf{H}\mathbf{x}^f\right). \qquad (2)$$

The length scale r_c is introduced such that correction from the surface observation is applied to the model forecast in the areas within the distance r_c from the top of the *D''*-layer r_d, i.e.

$$\mathbf{K} = \mathbf{0} \quad \text{if} \quad |r - r_d| > r_c. \qquad (3)$$

The numerical dynamo model used in our study is the MoSST core dynamics model developed at NASA GSFC [5], which is based on the original model developed by Kuang and Bloxham [6]. In this model, the magnetic field in the core is divided into the toroidal and poloidal components:

$$\begin{aligned}\mathbf{B} &= \mathbf{B}_T + \mathbf{B}_P \\ &\equiv \nabla\times\left(T_b\mathbf{1}_r\right) + \nabla\times\nabla\times\left(P_b\mathbf{1}_r\right),\end{aligned} \qquad (4)$$

where $\mathbf{1}_r$ is the radial unit vector, T_b and P_b are called the toroidal scalar and the poloidal scalar, respectively. In the MoSST core dynamics model, the two scalars are expressed in spherical harmonics,

$$\begin{bmatrix} P_b \\ T_b \end{bmatrix} = \sum_{0\le m\le l}^{l\le L} \begin{bmatrix} b_l^m(r) \\ j_l^m(r) \end{bmatrix} Y_l^m(\theta,\phi) + C.C. \qquad (5)$$

where b_l^m and j_l^m are called the poloidal and toroidal spectral coefficients, and *C.C.* means the complex conjugate. The spectral coefficients and their first order radial derivatives are defined on the radial grid points $\{r_i \mid i = 0, 1, 2\ldots N\}$.

The details of the optimal interpolation algorithm and the ensemble covariance algorithm shall be reported in separate manuscripts.

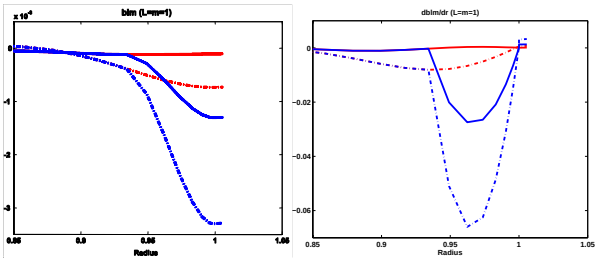

(a) (b)

Figure 1. The radial distribution of the model forecast (red) and the analysis (blue) defined by (2). In (a) are the real (the solid line) and the imaginary (dashed line) parts of the coefficient; and in (b) are the corresponding first order radial derivatives.

The OI developed in our model is very simple, and does not depend on the details of the model. An example for

the spectral coefficient b_1^1 of the poloidal field in the core is shown in Fig. 1.

In this example, $r_c \approx 0.07 r_{cmb}$ (r_{cmb} is the mean radius of the CMB). The scaling factor α is the ratio of the axial dipole coefficient b_1^0 of the forecast and of the analysis. The examples of the covariance curves are shown in Fig. 2.

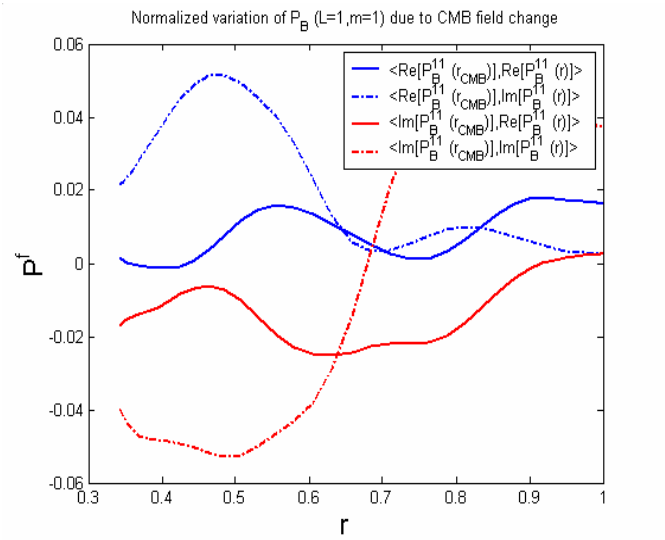

Figure 2. Examples of spatial covariance arrays in radius for the poloidal spectral coefficients. The correlation distributions are those between the coefficient b_1^1 *inside the core and itself on the CMB.*

Obviously the two distributions are very different. In particular, one can observe from Figure 2 that the correlation is significant throughout the entire outer core.

Our initial effort is focused on responses of the numerical model solutions to the constraints from the surface observations.

3. FIRST RESULTS OF GEOMAGNETIC DATA ASSIMILATION WITH THE OBSERVATIONS OVER THE PAST 100 YEARS

We have first tested the response of the numerical model to the constraints from the surface geomagnetic observations starting from 1900.

Geomagnetic field models [7] can provide poloidal spectral coefficients from surface (and near surface) observations. These coefficients can be downward continued to the top of the *D''*-layer r_d. In the MoSST model, a 20*km*-thick *D''*-layer is imposed at the top of the CMB r_{cmb}, i.e. $r_d = 20 + r_{cmb}$.

In our test, we only consider the field from the first 8 degree coefficients. For example, the radial component of the field is

$$B_r = \sum_{0 \le m \le l}^{l \le 8} \frac{l(l+1)}{r_d^2} b_l^m(r_d) Y_l^m + C.C. \qquad (6)$$

Also the magnetic free decay time τ_d is used for time scaling, i.e. the scaled time $\tau \equiv t/\tau_d$ for the observations matches that in the numerical model. For example, in the Earth's outer core, $\tau_d \approx 20000$ years. Therefore, a real time interval $\Delta t = 200$ years implies $\Delta\tau = 0.01$.

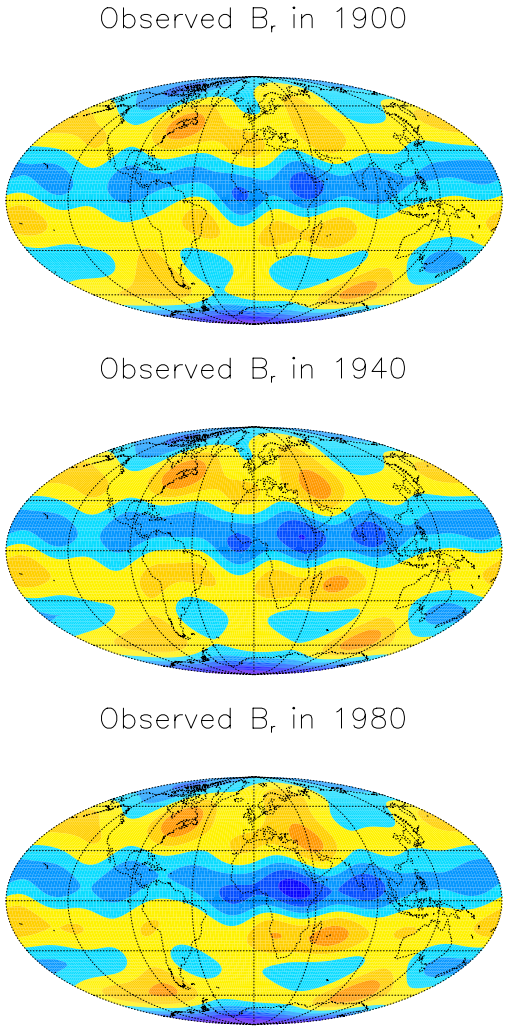

Figure 3. Snapshots of the modified radial component of the magnetic field $\widetilde{B}_r$ *(data provided by T. Sabaka).*

The scaling factor α in the numerical experiment is determined by the ratio of the axial dipole coefficients of the observation and of the forecast:

$$\alpha = \frac{b_1^{0(f)}}{b_1^{0(o)}}. \qquad (7)$$

Thus the axial dipole component is not assimilated , and since the dipole component is dominant in both surface observations and in numerical model outputs, the scaling (7) ensures that there is no significant field energy change before and after the analysis (2). Rescaling of state variables and/or observations is a standard practice in atmospheric data assimilation as a means to deal with complications in assimilation [8].

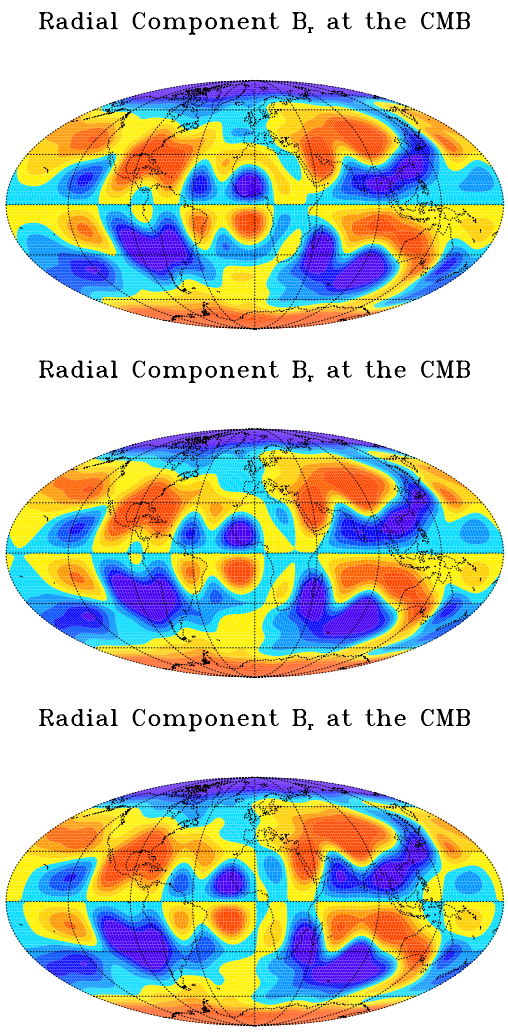

Figure 4. Similar to Fig. 3, but are the snap shots of the free model run (no assimilation). But the color scale in this figure is different from that in Fig. 3.

In Fig. 3, we show the snapshots of the modified (dipole-less) radial component of the magnetic field at the top of the *D"*-layer:

$$\widetilde{B}_r = \sum_{(l,m)\neq(1,0)} \frac{l(l+1)}{r_d^2} b_l^m(r_d) Y_l^m + C.C. \qquad (8)$$

From the figure one can observe clearly the small scale flux patches near the equatorial region.

The numerical model outputs without data assimilation (also called the free model runs) at the same epochs are shown in Fig. 4. From the figures one can easily observe that the free model runs are not at all similar to the observed field. In particular, the field morphologies are completely different. It should be pointed out here that the color scales in the figures are different, mainly to highlight the field configuration details.

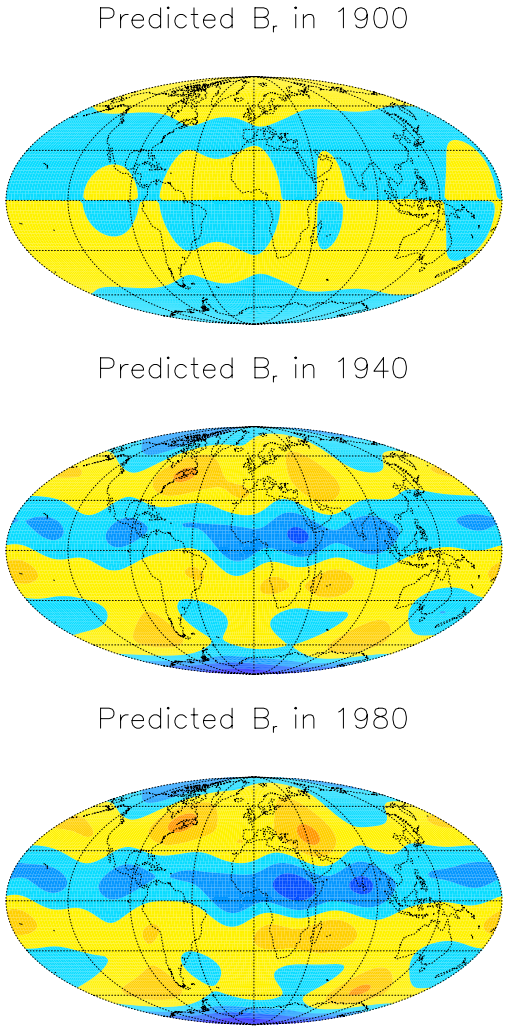

Figure 5. Similar to Fig. 3, but are the forecast results. The color scale is identical to that in Fig. 3.

The assimilation (2) is carried out at the interval $\Delta\tau$ = 0.001 (or every 20 years for the Earth's core). The analysis is then used as the initial state for the model simulation between the two assimilations. Between the

two assimilations, 4 forecasts are made for comparison with the observations. The examples of the forecast are shown in Fig.5.

From the figure one can observe clearly that the model forecasts are very different from the free model runs shown in Fig. 4. In particular, as the assimilation proceeds, the forecast is more similar to the observation. For example, the small scale field flux patches shown in the observation (Fig. 3) appear also in the forecast. This is particularly significant in the last panel of Fig. 5.

The similarity between the forecast and the observation can also be demonstrated by the r.m.s. of $\widetilde{B}_r$ at the top of the *D''*-layer, as shown in Fig. 6.

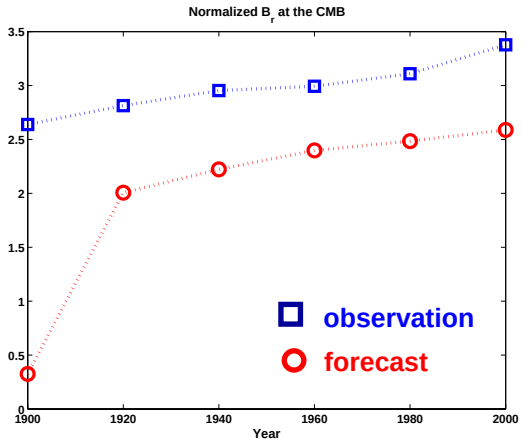

Figure 6. The r.m.s. of $\widetilde{B}_r$ for the observation (blue squares) and for the forecast (red circles) at the top of the D''-layer r_d.

While we can observe clearly the (positive) responses of the model to the surface observations from Figs. 5 and 6, we could not assess the responses of the model solutions inside the core to the observations, because the state variables inside the core are not observable, thus there is no reference for comparison. In addition, the surface observation record is too short in comparison with the geological time, thus perhaps insufficient for examining the spin-up time for the OI (e.g. the history of assimilation). To address these questions, we turn to synthetic assimilation.

4. SYNTHETIC ASSIMILATION EXPERIMENTS

The synthetic data are created from a free model run with a different Rayleigh number. For example, in one experiment, the numerical solutions with $R_2 = 15000$ are assumed to be the truth, and "synthetic" data are made from the solutions. The model with the Rayleigh number $R_1 = 14500$ is used for the forecast. The details of the synthetic data assimilation shall be reported separately. In this manuscript, we report some of the results related to our discussion.

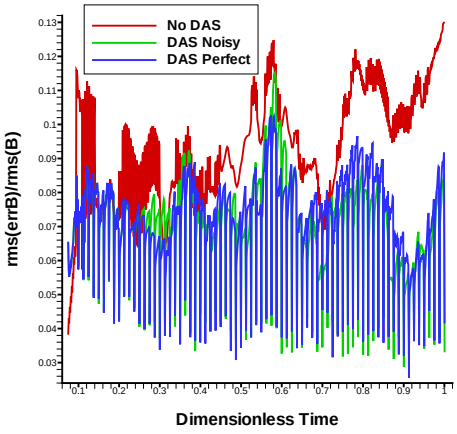

Figure 7. The differences between the poloidal field forecast and the truth in the vicinity of the CMB. The red line is the r.m.s. of the difference between the free model runs and the truth; the green line is that between the forecast (with noise added to the observation) and the truth; the blue line is that between the forecast (without noise in the observation) and the truth

Our synthetic assimilation experiment shows that spin-up time does affect the forecast significantly. In Fig. 7 we show the differences between the forecast and the truth of the poloidal field over the entire time domain. One can observe clearly that the difference between the forecast and the truth decreases with time, and is smaller than that between the free model run (no assimilation) and the truth. In addition, the longer the spin-up time, the smaller the difference, as shown in Fig. 8.

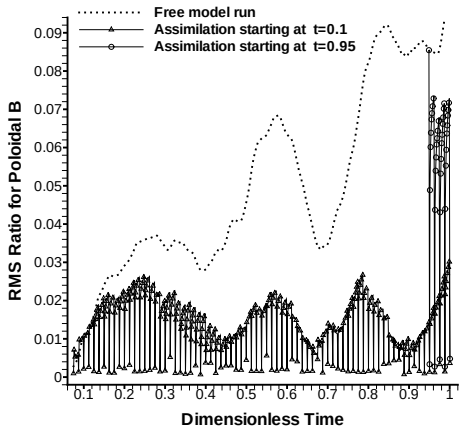

Figure 8. The difference between the forecast and the truth near the CMB with a 0.9 (non-dimensional) spin-up time (the triangles) and with a 0.05 spin-up time (squares).

The state variables that cannot be observed at the surface also respond to the constraints on the surface

observation. For example, in Figure 9 are the differences between the forecast of the toroidal field to the free model run, and between the forecast and the truth. From the figure we can observe that the difference between the forecast and the free model run increases in time. However, the difference between the forecast and the truth also increases in time, though at a slower rate. Thus the test results are insufficient to assess the responses of other state variables to the observed poloidal field.

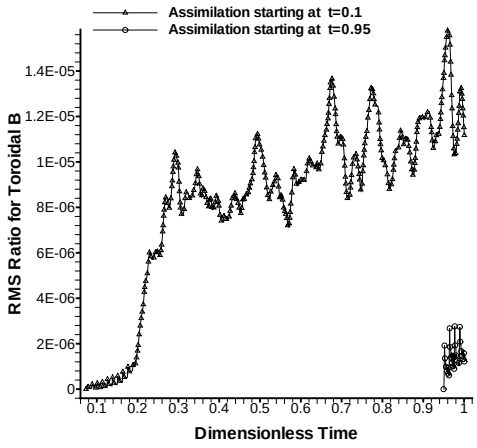

(a)

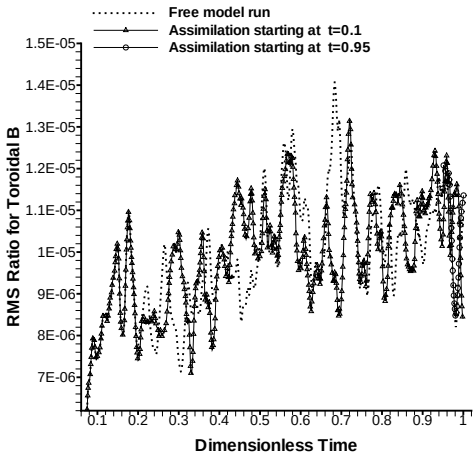

(b)

Figure 9. The difference (a) between the toroidal field forecast and the free model run, and (b) between the forecast and the truth.

5. DISCUSSION

In this paper we have discussed the algorithms we used for our geomagnetic data assimilation, and initial results from the test with 100-year surface geomagnetic observations, and from the synthetic data assimilation experiment.

Our results suggest that the numerical model does respond strongly to the constraint from surface poloidal field observations. While test results with the optimal interpolation algorithm clearly demonstrate positive responses of the poloidal field to the constraint, no clear assessment can be made to the responses of other state variables, e.g. the toroidal field.

This problem suggests that the ensemble covariance analysis can be more optimal: unlike the OI, other state variables are also corrected according to the correlations between the state variables inside the core and the poloidal field at the top of the *D"*-layer.

We shall continue our work in this direction with longer geomagnetic and paleomagnetic records.

ACKNOWLEDGEMENT

We thank T. Sabaka for providing field models for our assimilation studies. This research is supported by NSF Math/Geosciences program under Grant EAR0327875, by NASA Solid Earth Natural Hazard Program, NASA Earth Surface and Interior Program, and NASA Mars Fundamental Research Program.

REFERENCES

1. Kono, M. and P. H. Roberts, Recent geodynamo simulations and observations of the geomagnetic field, *Rev. Geophys.*, Vol. 40, 1-53, 2002.
2. Kuang, W. and J. Bloxham, An Earth like dynamo model, *Nature*, Vol. 389, 371 – 374, 1997.
3. Talagrand, O., Assimilation of observations, an Introduction, *J. Meteor. Soc. Japan*, Vol. 75, 191 – 209, 1997.
4. Berry P. J. and J.C. Marshall, Ocean studies in support of altimetry, *Dyn. Atmos. Oceans.*, Vol. 13, 269 – 300, 1989.
5. Kuang, W. and B. F. Chao, Geodynamo modeling and core-mantle interaction, in: Dehandt *et al* (eds) The core-mantle boundary region, *Geodynamics Series*, Vol. 31, 193-212, AGU, Washington, D.C., 2003.
6. Kuang, W. and J. Bloxham, Numerical modeling of magnetohydrodynamic convection in a rapidly rotating spherical shell: weak and strong field dynamo action, *J. Comp. Phys.*, Vol. 153, 51-81, 1999.
7. Sabaka, T. J., N. Olson and R. A. Langel, A comprehensive model of the quiet-time near-Earth magnetic field; phase 3., *Geophys. J. Int.* Vol. 151, 32-68, 2002.
8. Dee, D.P. and A.M. Da Silva, The choice of variable for atmospheric moisture analysis, *Month. Weath. Rev.* Vol. 131, 155-171, 2003.